Integrated Environmental Assessment and Management, 2026, 1–12
https://doi.org/10.1093/inteam/vjag003
Published: January 10, 2026
Original Article | Special Series

Comparative analysis of lignin peroxidase and laccase responses to graphene-related nanomaterials

Humberto Castillo-González[1,†], Fabio Candotto Carniel[2,*], Mario Mardirossian[2], Ester Vázquez[3,4], Maurizio Prato[1,5,6] and Mauro Tretiach[2]

[1]Department of Chemical and Pharmaceutical Sciences, University of Trieste, Trieste, Italy
[2]Department of Life Sciences, University of Trieste, Trieste, Italy
[3]Instituto Regional de Investigación Científica Aplicada (IRICA), Universidad de Castilla-La Mancha, Avda. Camilo José Cela, Ciudad Real, Spain
[4]Departamento de Química Inorgánica, Orgánica y Bioquímica, Facultad de Ciencias y Tecnologías Químicas, Universidad de Castilla-La Mancha, Ciudad Real, Spain
[5]Center for Cooperative Research in Biomaterials (CIC biomaGUNE), Basque Research and Technology Alliance (BRTA), Donostia-San Sebastián, Spain
[6]Ikerbasque, Basque Foundation for Science, Bilbao, Spain

*Corresponding author: Fabio Candotto Carniel. Email: fcandotto@units.it
[†]Present address: Université Marie et Louis Pasteur, CNRS, Chrono-environnement (UMR 6249), F-25200 Montbéliard, France.

Editor's Note: This article is part of the special series "RemTech Europe 2024: Comprehensive Approaches for the Management of Contaminated Sites." The series collects new frontiers to fighting and managing "old" and "new" contaminants that can be found in environmental sites.

Abstract

Graphene-related materials (GRMs) are revolutionizing sectors such as electronics, energy storage, agriculture, and biomedicine due to their exceptional properties. However, concerns are emerging about their environmental impact, particularly regarding their persistence, potential toxicity to aquatic ecosystems, and challenges in safe disposal. These issues highlight the need for more robust sustainable-by-design and risk-assessment strategies. In this context, this research investigated the influence of GRMs on lignin peroxidase (LiP) and laccase (Lac), key enzymes involved in lignin breakdown with significant potential in bioremediation. These enzymes are crucial for degrading complex molecules, and understanding their interaction with GRMs could provide valuable insights into the degradation of 2D nanomaterials, particularly graphene oxide (GO), few-layer graphene (FLG), and reduced graphene oxide (rGO). In vitro enzymatic assays conducted with varying GRMs concentrations (12.5, 25.0, and 50.0 μg/mL) revealed that Lac remained unaffected, while LiP exhibited a noteworthy reduction in catalytic activity, particularly in the presence of GO at the highest concentration. A sequestration study to quantify the bioavailable fraction confirmed these effects, indicating significant enzyme loss, notably with GO at 50 μg/mL. These findings prompted a mechanistic exploration of enzyme inhibition dynamics, revealing the complex nature of GRM-catalytic enzyme processes. By considering factors such as zeta potential (electrostatic forces), hydrophobicity, dispersion stability, and oxidation state, this study addresses a key knowledge gap and provides a foundation for understanding these interactions, offering crucial insights into the environmental fate of GRMs and guiding their sustainable use and management.

Keywords 2D nanomaterials, electrostatic interactions, enzyme sequestration, fungal lignolytic enzymes, zeta potential

Introduction

The emergence of 2D nanomaterials (2DNMs), exemplified by graphene oxide (GO), reduced graphene oxide (rGO), and few-layer graphene (FLG), has ushered in a transformative era across various industries, fueling innovations in electronics, energy storage, sensing devices, agriculture, and biomedical applications (Das et al., 2023; Goodrum et al., 2024; Malisz & Świeczko-Żurek, 2023; X. Zhang et al., 2022). Despite these strides, concerns loom over the biodegradability of these materials. While some studies hint at potential biodegradation (Fan et al., 2017; Liu et al., 2022b; H. Yang et al., 2019), the long-term environmental impact, including toxicological effects and ecosystem mobility, remains inadequately understood (Ding et al., 2022; Evariste et al., 2021; Martín-De-Lucía et al., 2018; Ye et al., 2018). Striking a delicate balance between the substantial benefits afforded by 2DNMs and a comprehensive understanding of their environmental risks is imperative for their responsible and sustainable integration into diverse applications.

Received: March 28, 2025. **Revised:** November 25, 2025. **Accepted:** December 30, 2025.

Recent studies have explored the biodegradation of 2DNMs, with particular attention to their interactions with fungi and bacteria (Candotto Carniel et al., 2021; Qu et al., 2018; H. Yang et al., 2018). Fungi, particularly white-rot species such as *Phanerochaete chrysosporium*, stand out for their ability to break down recalcitrant materials, underscoring their potential in environmental remediation (Madenli & Deveci, 2023). This capacity is attributed to both extracellular enzymes, such as laccases and various peroxidases, and intracellular systems, including the cytochrome P450 family (CYP), epoxidases, and transferases (A. Kumar & Chandra, 2020). Among the former, lignin peroxidase (LiP) and laccase (Lac) stand out for their activity and are known to degrade complex structures, potentially including graphene-related nanomaterials (GRMs). This biotransformation is hypothesized to occur via the generation of highly reactive radicals by LiP, and through the direct oxidation of functional groups and aromatic domains by Lac. If successful, these enzymes could offer a sustainable strategy for targeted degradation or, at minimum, provide insights into the intricate processes governing the environmental fate of GRMs. However, further research is needed to fully understand 2DNMs and guide their responsible application across diverse environmental and technological domains.

Lignin peroxidase, a heme-containing oxidoreductase, is renowned for catalyzing the H_2O_2-dependent oxidative depolymerization of lignin (Barnhart-Dailey et al., 2019; A. Kumar & Chandra, 2020), i.e., the complex polymer that provides structural support to plant cell walls (Martinez et al., 2022). This oxidative capacity stems from its ability to generate highly reactive radicals, enabling it to attack stable carbon–carbon bonds, particularly in aromatic structures (Barnhart-Dailey et al., 2019). Conversely, Lac, a member of the multicopper oxidase family, catalyzes the oxidation of a variety of substrates, including phenolic compounds, generating reactive radicals that contribute to lignin degradation (W. Zhang et al., 2021). Unlike LiP, which relies on H_2O_2 for its oxidative activity, Lac uses molecular oxygen as an electron acceptor, diversifying the oxidative mechanisms involved in lignin depolymerization. The versatile and collaborative interplay between LiP and Lac in certain fungi forms an adept enzymatic system, whose oxidative capacity extends beyond lignin to degrade a wide range of recalcitrant macromolecules (Kantharaj et al., 2017), including synthetic polymers, and potentially graphene-related materials, contributing to their detoxification and limiting their accumulation in ecosystems. Unfortunately, despite substantial progress, achieving complete biodegradation of GRMs remains challenging, attributable to factors such as heterogeneity in their physicochemical properties and variations in enzymatic activities (Fojtů et al., 2017; Kenry & Lim, 2017; Shams et al., 2023; Xie et al., 2016).

This study builds on prior research, specifically Fortuna et al. (2023), who reported unexpected inhibition of LiP during GRM biodegradation by *P. chrysosporium*, a finding that warrants deeper investigation. The present study aims to validate this inhibition, explore the interaction-driven factors underlying this phenomenon, and further examine/discuss the role of Lac in GRM biodegradation. Focusing on these objectives, the study fills an important knowledge gap, providing foundational insights to guide future research and to inform strategies for the safe management of GRMs in the environment.

Materials and methods

Materials

Acetate buffer 0.1 M at pH 4.5 was prepared for all reactions involving Lac to optimize enzyme activity. For LiP, a buffer consisting of tartaric acid (TA 10 mM)–sodium tartrate (Na-Ta 30 mM) (50:13 v/v) at pH 3.2 was chosen to simulate natural slightly acidic conditions. Lignin peroxidase powder form was obtained from Creative Enzymes (Shirley, NY, USA), while Lac was sourced from Sigma (St. Louis, MO, USA). Graphene oxide (GO) and reduced GO (rGO) were sourced from Graphenea (San Sebastián, Spain), and few-layer graphene (FLG) was prepared via ball-milling as described by González-Domínguez et al. (2018), starting from a mixture of graphite (7.5 mg of SP-1 graphite powder, Bay Carbon) and melamine (22.5 mg of 1,3,5-triazine-2,4,6-triamine; Sigma-Aldrich, Saint Louis, Missouri, US). The resulting solid mixture was suspended in water, and melamine was washed away by dialyzing against water.

All nanomaterials were dispersed at concentrations of 12.5, 25.0, and 50.0 μg/mL in their buffers, with 0.0 μg/mL serving as a control. Solid GRMs were dispersed through high-speed vortexing followed by alternating 10-second sonication cycles in a Selecta ultrasonic cleaning bath (model no. 3000513; J.P. Selecta, Barcelona, Spain), set to 50/60 Hz frequency and 360 W nominal power, interspersed with brief manual shaking for a total of 1 minute. Graphene oxide was acquired in liquid form. The materials were thoroughly characterized as reported in Fortuna et al. (2023). Briefly, GO and rGO were analyzed by the manufacturer using a LECO CHNS-932 analyzer (LECO Corporation, St Joseph, MI, USA) to determine the content of carbon (C), hydrogen (H), nitrogen (N), and sulfur (S). Particle dimensions, including lateral size and thickness, were evaluated using laser diffraction, high-resolution transmission electron microscopy (HR-TEM JEOL 2100, JEOL, Tokyo, Japan), and environmental scanning electron microscopy (ESEM, Quanta 250 FEG, FEI, Brno, Czechoslovakia). Few-layer graphene powder was characterized by thermogravimetric analysis (TGA), Raman spectroscopy, and electron microscopy to assess structure and morphology following González et al. (2020; see online supplementary material Figure S2).

Enzyme-substrate reactions

All enzymatic reactions were performed in triplicate at room temperature (∼25 °C). Reactions were designed as endpoint measurements across GRM concentrations, as continuous time-course kinetics were precluded by optical interference from GRMs.

For laccase activity, reactions contained 65.4 μM ABTS (2,2'-azino-bis (3-ethylbenzothiazoline-6-sulfonic acid)) and 150.0 μg/mL Lac, with GRM concentrations of 12.5, 25.0, or 50.0 μg/mL, in acetate buffer. The final reaction volume was adjusted to 600 μL and the reaction was incubated for 10 min. For lignin peroxidase, reactions contained 150 μg/mL LiP and 8.4 mM veratryl alcohol (VA) with GRM concentrations as above, in TA/Na-Ta buffer. The reaction was initiated by adding hydrogen peroxide (0.84 mM H_2O_2). The final volume was adjusted to 1 ml, and the reactions were incubated for 40 minutes. After incubation, all samples were filtered through 0.22 μm syringe filters to remove GRMs prior to absorbance measurements, preventing optical interference. Substrate conversion was quantified by measuring absorbance at the respective maximum wavelengths for product formation: 734 nm for $ABTS^{\cdot+}$ (Lac) and 310 nm for oxidized VA (LiP). All absorbance measurements were blank-corrected using the corresponding buffer

without enzyme or substrate. Absorbance was measured in quartz cuvettes with a 1 cm pathlength and 2 mm internal width (0.5 mL working volume) using a Jenway 7415 UV/VIS spectrophotometer (Cole-Parmer, Vernon Hills, Illinois, US).

Separately, to evaluate GO oxidation through the qualitative assessment of hydrogen peroxide (H_2O_2) production, the Amplex Red assay from Thermo Fisher Scientific (Waltham, MA, USA) was performed following the manufacturer's instructions. After incubating 150 μg/ml Lac with 50.0 μg/ml GO for 24 and 48 hours, samples were diluted in 1X reaction buffer, combined with the Amplex Red Working Solution, and incubated at room temperature for 30 minutes, protected from light. Controls without enzyme were included to account for nonenzymatic H_2O_2 formation.

Enzyme entrapment

To detect enzyme sequestration, 150 μg/ml of each enzyme was incubated with GRMs at concentrations of 12.5, 25.0, or 50.0 μg/ml in their respective buffers. Incubation times mirrored those of the enzyme-substrate reactions: 40 minutes for LiP and 10 minutes for Lac. To eliminate nanoparticles and ensure solution clarity for subsequent spectrophotometric analyses, initial attempts to filter the nanoparticle-enzyme solution using 0.22 μm filters were made. However, these attempts were hindered, because the filter not only blocked nanoparticle passage but also trapped the proteins. Therefore, ultracentrifugation (UC) was performed using a Himac CS150NX ultracentrifuge equipped with an S50A rotor (Hitachi, Tokyo, Japan) at 150,000 rpm for 25 minutes at room temperature and it was employed to remove GRMs, eliminating both optical and chemical interference in downstream assays.

Protein concentrations in the post-UC supernatants were quantified using the bicinchoninic acid (BCA) assay (Novagen BCA Protein Assay Kit, Merck, Darmstadt, Germany). Following the manufacturer's enhanced protocol, these samples were incubated with the BCA working reagent at 60 °C for 15 min prior to absorbance measurement at 562 nm using a Jenway 7415 UV/VIS spectrophotometer (Cole-Parmer, Vernon Hills, Illinois, US). Calibration curves were prepared in the corresponding enzyme buffer over a concentration range of 5–250 μg/ml, without spiking with GRMs, considering UC effectively removed nanomaterials prior to measurement. Linear regression of absorbance against standard concentration was performed to determine the slope, intercept, and coefficient of determination (R^2), which were then used to calculate protein concentrations in the samples. Standard calibration curves, including regression equations and R^2 values, are provided in online supplementary material Figure S2.

Zeta potential

Zeta potential (ζ-potential, ZP) was measured to characterize the surface charge of GRMs and their interactions with LiP. Samples containing each GRM at three concentrations were prepared in TA/Na-Ta buffer, with or without 150 μg/mL LiP (incubated 40 minutes at room temperature). Measurements were conducted in triplicate using a Malvern Zetasizer NANO-ZS (Malvern Panalytical, Malvern, U.K.), equipped with a 4 mW 632.8 red laser. Samples (1.0 mL) were placed in clean polystyrene cuvettes and analyzed at room temperature. Results were averaged over the three repetitions.

Data processing, statistical analyses, and visualization

All analyses were performed in R (version 4.5.2) within RStudio. For enzyme-substrate reactions, assays absorbance (Abs) was converted to concentration using the Beer–Lambert law:

$$C(\mathrm{mM}) = \frac{\mathrm{Abs}}{\varepsilon \cdot \ell} \times 1000,$$

where ε is the molar extinction coefficient (LiP: $\varepsilon = 9{,}300\ \mathrm{M}^{-1}\ \mathrm{cm}^{-1}$; Lac: $\varepsilon = 15{,}000\ \mathrm{M}^{-1}\mathrm{cm}^{-1}$) and $\ell = 1$ cm.

Fold-change relative to the mean control concentration was calculated per replicate as:

$$\mathrm{Fold\ Change}_i = \frac{C_i}{C_{control}}$$

and percentage of protein remaining was calculated as:

$$\%\ \mathrm{Protein\ remaining} = \frac{Protein_{sample}}{Protein_{control}} \times 100$$

For each treatment group (n = 3), we assessed normality of residuals using the Shapiro–Wilk test (performed by group where appropriate). Potential outliers were screened with Grubbs' test applied within each treatment group. Model residuals were also inspected graphically (histograms and residual plots) given the small group size.

When normality and absence of influential outliers were met, differences among treatments were tested with one-way ANOVA (response ~ Treatment). For ζ-potential, which involves two factors (material × concentration), two-way ANOVA with interaction was used (response ~ Treatment * Concentration). Where ANOVA indicated a significant main effect or interaction ($\alpha = 0.05$), Dunnett's test was used for a priori comparisons of each treatment versus control (one-way ANOVA analyses), and Tukey's Honest Significant Difference (HSD) was used for all pairwise comparisons following two-way ANOVA. In addition, pairwise *t*-tests with Holm/Holm-Bonferroni correction were used for within-group comparisons where indicated. All multiple comparisons controlled family-wise error rate.

For each ANOVA model, we computed and report F-statistics, *p*-values, and effect sizes (η^2 and ω^2), together with Shapiro–Wilk *p*-values. All statistical outputs are provided in online supplementary material Tables S1–S3.

Plots were generated with ggplot2 (boxplots, point/error-bar plots with annotated significance). Specific R packages used in the analysis include ggplot2, DescTools (DunnettTest), multcomp (glht, Dunnett contrasts), and base R stats for aov, TukeyHSD, shapiro.test, and pairwise.t.test.

Results

GRM characterization

The main physicochemical properties of the GRMs are presented in Table 1. Few-layer graphene exhibited submicron to micron-scale lateral dimensions and a predominantly carbonaceous composition, rGO displayed intermediate oxygen content and larger particle sizes, and GO showed the highest oxygen content within the series. Online

Table 1 Particle size and elemental composition of FLG, rGO, and GO.

GRM	Particle size (μm)	Elemental composition (%)				
		C	H	N	S	O
FLG	0.1–1	95.56	0.33	0.2	0.33	0.24
rGO	1–15	80–87	0–1	0–1	0–1	13–17
GO	<10	49–56	1–2	0–1	2–3	41–50

Note. FLG = few-layer graphene; rGO = reduced graphene oxide; GO = graphene oxide.

supplementary material Figure S1 shows the Raman and microscopy data for FLG.

Effect on enzyme activity

The impact of different concentrations of GRMs on enzyme activity was assessed. At a concentration of 50 μg/ml, all GRMs notably affected the activity of lignin peroxidase. Graphene oxide exhibited the most significant inhibitory effect, resulting in a deceleration of the LiP and veratryl alcohol reaction (Figure 1A). In contrast, Lac activity remained unaffected in the presence of GRMs, with no significant differences in product accumulation compared to the control (p = .136) (Figure 1B). Additionally, the Amplex Red assay, used to detect hydrogen peroxide (H_2O_2) production, showed a colorimetric change from colorless to reddish in all samples except the control, confirming the presence of this reactive oxygen species (ROS).

Sequestration study

To investigate if the decline in enzymatic activity could be ascribed to enzyme sequestration rather than specific inhibition, an assay was set up to estimate the potential of GRMs to clear the enzyme from the solution. The sequestration study revealed pronounced sequestration of LiP across all concentrations of GO. Significant changes were also observed at the highest concentration of FLG (50 μg/ml) and rGO (Figure 2A). In contrast, the concentration of Lac after incubation with the nanomaterials exhibited no significant difference in the treatment groups compared to the control (p = .997; Figure 2B).

ζ-potential

As shown in Figure 3, results consistently demonstrated a high negative zeta potential for all GRMs, with GO exhibiting particularly pronounced values. Notably, there was a transition toward the positive spectrum after the nanomaterials were incubated with the enzyme. A discernible trend of increased ζ-potential, reflecting higher negative values for GRMs alone and higher positive values for GRMs + LiP with escalating concentrations, was evident across all materials. This trend reached statistical significance, particularly in the case of rGO alone.

In the case of the GRMs alone, statistical analyses underscored noteworthy differences between treatments, specifically GO-FLG (p = 1.4e-10) and GO-rGO (p = 4.6e-10). However, no statistically significant distinction emerged between rGO and FLG ($p > .05$). Within individual treatments, the ζ-potential did not significantly change between concentrations of GO or FLG (p values >.05). In contrast, within the rGO group, significant differences were identified among all concentrations (μg/ml), specifically between 12.5 and 25 (p = .01008), 25 and 50 (p = .00300), and 12.5 and 50 (p = .00028).

Upon the addition of LiP to the GRMs, significant differences between GO-FLG (p = .0429485) and rGO-GO (p = .0005125) were revealed. Concentration affected the ζ-potential between GO 12.5–50 (p = .032) and rGO 12.5–50 (p = .0062). Conversely, no significant differences were observed in the case of FLG for any concentration.

Discussion

By examining how graphene-related materials interact with key oxidative fungal enzymes, we found that their effects are highly material-dependent. Graphene oxide at 50 μg/ml, in particular, markedly inhibited LiP activity, resulting in a significant reduction of product formed (Figure 1), indicating that this material can interfere with ligninolytic catalysis. In contrast, Lac activity remained unaltered under the same conditions. The test concentrations used here were chosen to probe mechanistic and sublethal responses under controlled laboratory conditions and are in the range of, or slightly higher than, those used in prior mechanistic and ecotoxicological investigations of graphene-family nanomaterials (Goodwin et al., 2018; Németh et al., 2023; Zhang et al., 2024). While 50 μg/ml exceeds concentrations typically expected in bulk environmental compartments (e.g., predicted concentrations in surface waters are in the ng/L range), material-flow modeling and predicted environmental concentration (PEC) studies indicate that localized hotspots, e.g., accumulation in wastewater-treatment plant sludge, soils following sludge application, or direct agricultural amendments, can reach substantially higher concentrations in soils or local aqueous microenvironments, making our results environmentally relevant (Hong & Nowack, 2024; Keller & Lazareva, 2014; Zhao et al., 2021). This is especially pertinent given that our sequestration study revealed persistent interactions between LiP and GO across all tested concentrations, with additional effects observed for FLG and rGO at the highest doses tested (Figure 2). Together, these findings underscore the complexity of GRM–enzyme interactions, offering valuable insights for future studies in the realms of nanobiotechnology and environmental science.

The physicochemical properties of graphene related nanomaterials, including surface charge, size, and functional groups, dictate their interaction with enzymes (Kenry & Lim, 2017; Mokhtari-Farsani et al., 2022). Graphene oxide exhibits a hexagonal lattice structure with oxygen-containing functional groups on its basal plane and edges. Unlike pristine graphene, these groups create heterogeneity and hydrophilicity, enhancing GO's dispersibility in aqueous solutions. Oxygen groups include epoxides, hydroxyls, and carboxyls, which foster the formation of C–OH bonds and influence GO's reactivity (Yu et al., 2020). In aqueous environments, some functional groups ionize, releasing protons (H^+) and generating a negatively charged surface, e.g., carboxylates (–COO^-; Nidamanuri et al., 2020; Zhang et al., 2019). The diverse functional groups also serve as binding sites for proteins, facilitating sequestration (Kumar & Parekh, 2020; Wojciechowska et al., 2023), which appears to increase at higher concentrations, possibly due to more available binding sites or altered GO aggregation patterns. At pH 3.2, LiP carries a net positive charge, promoting attraction to the negatively charged surface of GO, whereas at pH 4.5, Lac is negatively charged and may experience repulsion.

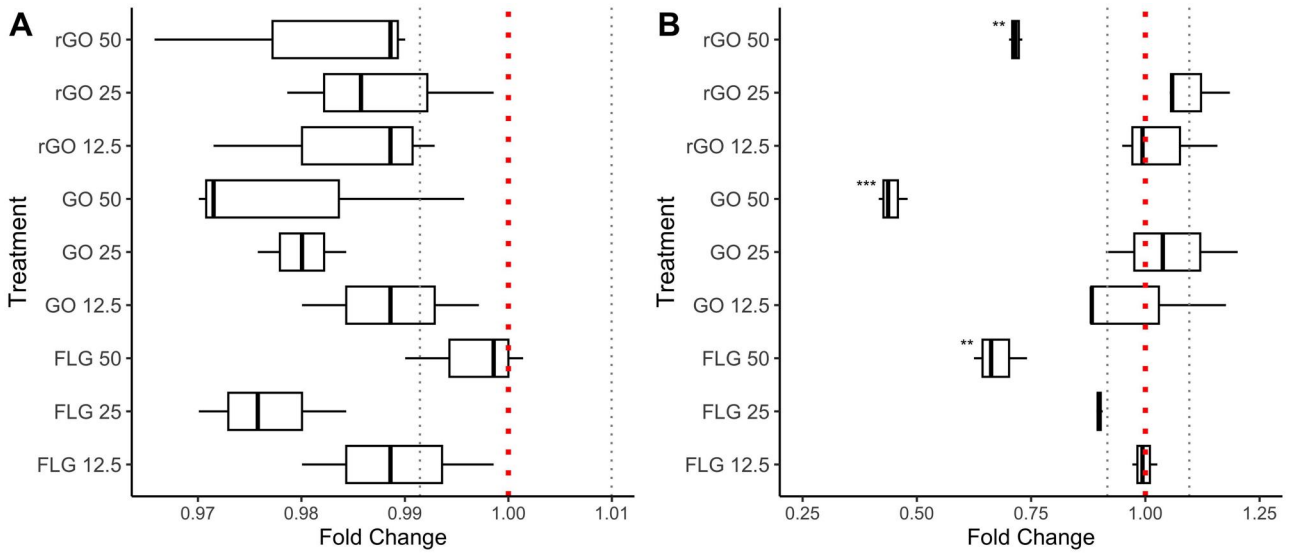

Figure 1 Fold-change in product formation relative to control following interaction with graphene-related materials for (A) laccase and (B) lignin peroxidase. The red dotted line indicates the control baseline (fold-change = 1), and gray dotted lines show the observed variation among control replicates. Asterisks denote significant differences from control (Dunnett's post hoc test). *Note*. rGO = reduced graphene oxide; GO = graphene oxide; FLG = few-layer graphene.

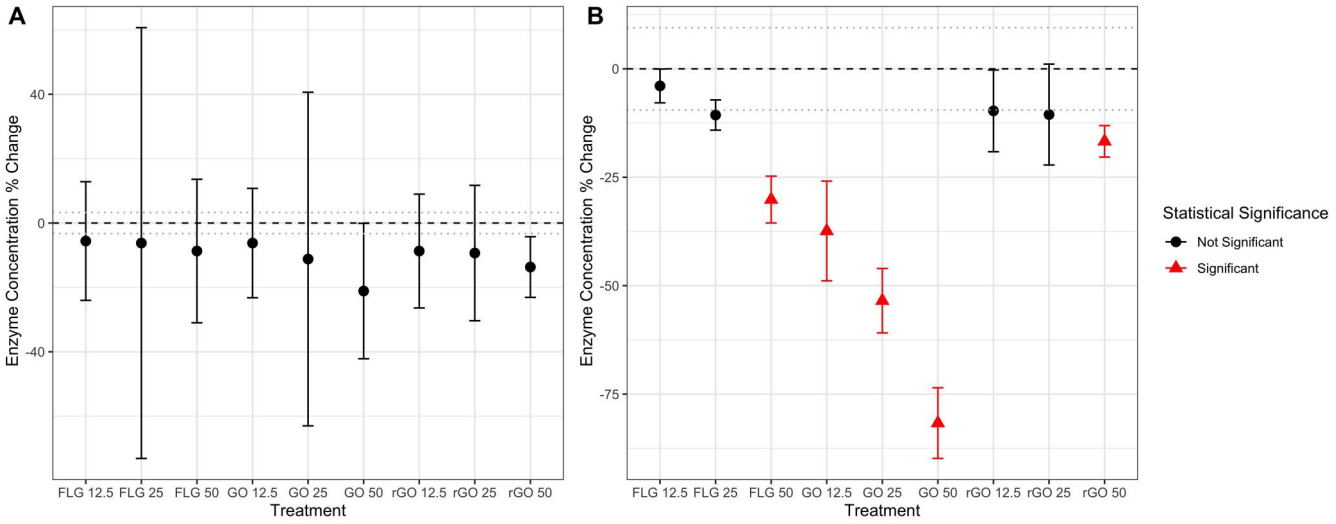

Figure 2 Percentage change relative to control in bioavailable enzyme concentration following graphene-related material interactions for (A) laccase and (B) lignin peroxidase, with gray dotted lines showing the 95% CI of the control. Error bars represent 95% confidence intervals. Significant differences were determined via Dunnett's test ($p < .05$). *Note*. rGO = reduced graphene oxide; GO = graphene oxide; FLG = few-layer graphene.

These observations suggest that electrostatic interactions constitute the primary mechanism of enzyme–GO association. Further investigation of pH and ionic-strength effects is warranted, as variations in catalytic activity may reflect intrinsic pH-dependent properties. Zeta potential measurements corroborate electrostatic binding as a key interaction mechanism (Figure 3): all GRMs exhibit negative surface charges in solution, which shift to positive values upon LiP adsorption, indicating surface coverage by the positively charged enzyme. The absolute shift is greatest for GO, significantly exceeding the shift observed for the less functionalized FLG and rGO, reflecting GO's high density of negatively charged functional groups, which provide more binding sites for the enzyme, leading to a more dramatic charge reversal.

Moreover, the ZP of rGO alone exhibits a clear concentration dependence, becoming more negative as particle concentration increases. This trend is likely driven by concentration-enhanced aggregation, where intersheet stacking modifies the exposed surface charge at the shear plane of the resulting aggregates. When rGO is subsequently mixed with the enzyme, adsorption of positively charged LiP partially neutralizes the surface charge, producing the observed positive ZP shift that is also dependent on rGO concentration. Within each GRM, higher particle loading introduces a larger

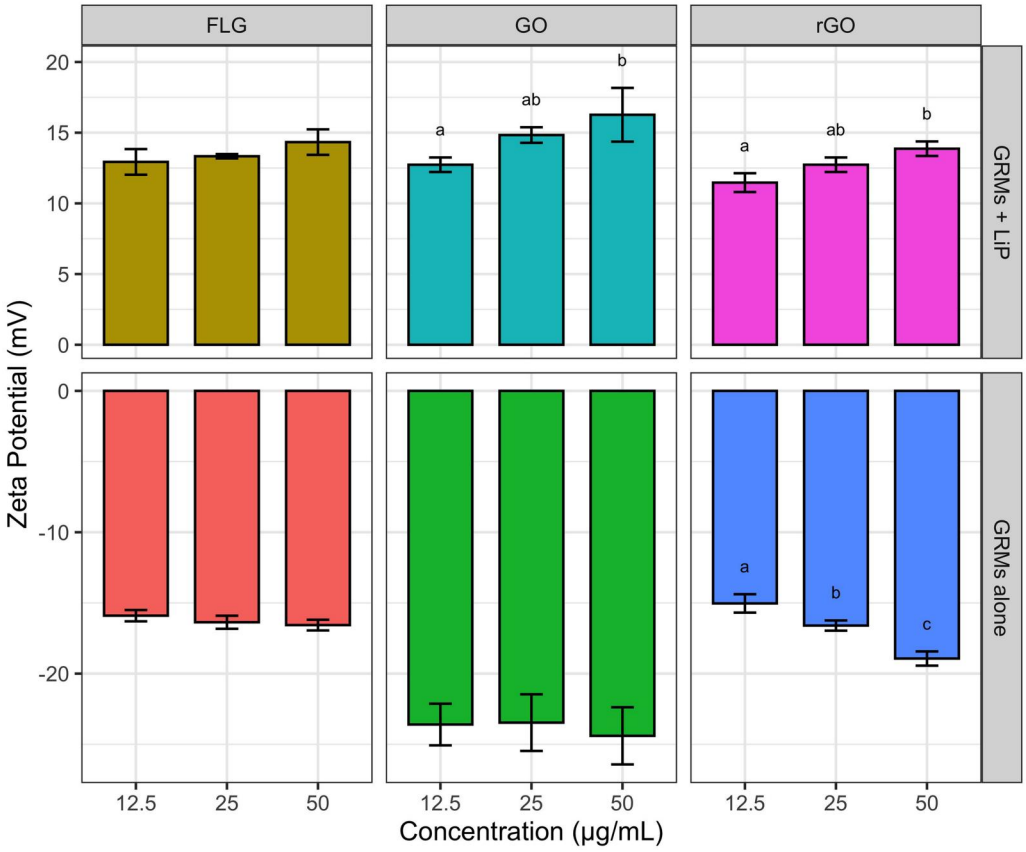

Figure 3 Zeta potential (mV) of graphene-related materials at various concentrations, measured in isolation and after incubation with lignin peroxidase. Different letters indicate statistically significant differences ($p < .05$). *Note*. GRMs = graphene-related materials; LiP = lignin peroxidase; rGO = reduced graphene oxide; GO = graphene oxide; FLG = few-layer graphene.

total nanomaterial surface, even if some aggregation occurs, and this provides more binding sites for the enzyme. Our results are consistent with this mechanism, reflecting the development of enzyme–GRM complexes that mask the intrinsic surface charge. Together, these findings support the interpretation that enzyme inhibition at higher GRM concentrations arises from surface adsorption and partial shielding of the enzyme's active site.

However, between different GRMs, the effect of intrinsic surface area is harder to predict, partly because apparent surface differences must be interpreted in light of our dosing scheme, which is based on mass concentration (μg/ml). Reported Brunauer-Emmett-Teller (BET) values for graphene-family materials vary widely depending on synthesis and post-treatment. For example, GO and rGO can exhibit surface areas ranging from tens to several hundred m^2/g (Guo et al., 2014; Karaphun et al., 2021; Lee et al., 2013), while activated or templated rGO can reach ~1,000–3,000 m^2/g (Boulanger et al., 2022; Wang et al., 2015), and FLG spans a few hundred to over 2,000 m^2/g (Islam et al., 2021; Purkait et al., 2017). If activity or inhibition were simply proportional to surface area (apparent trend: FLG > rGO > GO), the material with the highest surface area would be expected to exhibit the strongest effect; however, this was not observed. Critically, however, BET values measured under dry nitrogen do not necessarily correspond to the surface area accessible to enzymes or other macromolecules in aqueous environments where sheet folding, restacking, aggregation and morphology changes (Ali et al., 2023; Jiang et al., 2016), substantially reduced solvent-accessible surface area, and even liquid-phase dye-adsorption methods can be influenced by these structural dynamics (Chen et al., 2020; Ortiz-Anaya & Nishina, 2024). Thus, while differences in accessible surface area likely contribute to the material-specific patterns we observe, mass-normalized comparisons remain appropriate for the exposure context of this study.

In addition to surface-area considerations, molecular size also shapes enzyme–GRM interactions. Lignin peroxidase (~40 kDa) is substantially smaller and more compact than Lac (~60–80 kDa; Fortuna et al., 2023), which enables closer approach to nanomaterial surfaces and reduces steric hindrance during adsorption. Smaller proteins also diffuse more rapidly in aqueous media, increasing the probability of productive collisions with exposed functional groups or defect sites on GRMs. While these size effects may favor interactions with the highly functionalized surface of GO, increasing the mass concentration of GRMs elevates the total number of accessible binding sites across all materials, including FLG and rGO. Under these conditions, concentration-dependent aggregation or partial exfoliation can further modulate the effective surface presented to proteins. The combined influence of enzyme size, surface heterogeneity, and concentration-driven changes in GRM dispersion is consistent with the inhibition of LiP activity observed at higher loadings of FLG and rGO, where enzyme sequestration becomes increasingly likely.

Nonetheless, rGO and FLG have fewer oxygen-containing groups than GO (Table 1), resulting in fewer protonable sites and a more stable, less negative surface charge, particularly under acidic conditions, which is reflected in the lower magnitude of their zeta potential

(Figure 3). The reduction in surface charge is coupled with an increase in intrinsic electrical conductivity across the materials' bulk, as the restoration of the sp^2 carbon network allows for efficient electron flow (Fadil et al., 2019; Henriques et al., 2020; Liu et al., 2022a; Van Khai et al., 2013). Furthermore, the higher inherent electrical conductivity of rGO and FLG increases the ionic strength at the interface, which compresses the Electrical Double Layer (EDL) and contributes to the lower ZP magnitudes observed (Figure 3). These less oxygenated materials, therefore, enable more efficient local electron redistribution, a property critical for applications such as enzyme catalysis, biosensing, and bioelectrocatalysis. Notably, LiP catalyzes veratryl alcohol via short-range, enzyme-bound single-electron transfer (Houtman et al., 2018), making its activity sensitive to the immediate interfacial environment. Consistent with this, rGO's higher conductivity has been shown to stabilize peroxidases and facilitate local redox cycling, acting as a mediator for electron flow without denaturing the enzyme (Zhang et al., 2015), which helps explain the reduced inhibitory effect of rGO and FLG on LiP-mediated catalysis compared to GO, which perturbs interfacial electron transfer more strongly.

It is noteworthy that, in our experiments, Lac did not exhibit the same inhibitory response observed for LiP. Moreover, in the presence of the highest GO concentration, where LiP showed clear inhibition, the Amplex Red assay revealed a color shift from colorless to red, indicating Lac-mediated oxidation of functional groups on the GRM. The detected H_2O_2 formation suggests that laccase engages in a noncanonical catalytic pathway when interacting with GO. Under typical conditions, Lac reduces O_2 to water via a four-electron transfer coupled to the oxidation of phenolic substrates:

$$4\,\mathrm{Phenol}_{\mathrm{red}} + O_2 \rightarrow 4\,\mathrm{Phenol}_{\mathrm{ox}} + 2\,H_2O$$

However, GO contains redox-active hydroxyl, carbonyl, and quinone-like groups within its partially reduced π-system, which can serve as unintended electron donors. Interaction of Lac with these surface moieties can drive incomplete oxygen reduction, producing H_2O_2 through a two-electron pathway:

$$GO + O_2 \overset{\mathrm{Lac}}{\rightarrow} \mathrm{GO}_{\mathrm{ox}} + H_2O_2$$

In this scenario, GO acts as a pseudo-substrate or redox partner rather than an inhibitor, enabling ROS formation without diminishing Lac activity. This behavior contrasts with that observed for LiP and highlights that GRM–enzyme interactions are highly enzyme-specific, governed not only by adsorption processes but also by the alignment between each enzyme's redox mechanism and the electronic and functional landscape of the nanomaterial surface.

Acknowledging these enzyme-specific responses emphasizes the inherent complexity and selectivity of GRM–enzyme interactions. Each enzyme engages with nanomaterials, through a distinct combination of adsorption behavior, redox compatibility, and kinetic constraints, which can lead to strikingly different outcomes. For laccase, its faster catalytic turnover relative to LiP likely reduces the effective contact time between the enzyme and the material, thereby limiting the window during which inhibitory interactions can occur. This underscores the importance of reaction kinetics and time-dependent processes when interpreting enzyme–nanomaterial behavior (Kumari et al., 2020). In this study, each assay was performed within the respective linear range of product formation. This means that both enzymes were evaluated at time points that reflect their intrinsic catalytic output in the absence of GRMs, making the comparison focused on interaction propensity rather than raw reaction rates. Thus, the contrast we draw refers specifically to the effective window for enzyme–material contact, not to absolute activity values.

Furthermore, other properties of GRMs, such as dispersibility and agglomeration, could impact the enzyme microenvironment and activity. Graphene oxide, for example, exhibits superior dispersibility and is obtained in liquid form (Caorsi et al., 2025), whereas FLG and rGO are more prone to aggregation. The heightened dispersibility and reduced agglomeration of GO likely enhances its electrostatic accessibility for LiP adsorption, facilitating sequestration, whereas aggregated FLG and rGO may reduce the number of functional surfaces exposed and available for enzyme interaction. Indeed, the highly negative zeta potential observed for GO sheets (Figure 3) suggests robust electrostatic repulsion between sheets, contributing to better colloidal stability and reduced tendencies for agglomeration (Gumustas et al., 2017), whereas lower ZP values favor van der Waals-driven stacking, coagulation, flocculation, or precipitation (Shnoudeh et al., 2019). In these cases, the nonsoluble rGO and FLG may inadvertently create a microenvironment that fosters enhanced enzyme activity, because reduced obstruction within the reaction milieu allows enzymes easier access to substrates such as VA or ABTS, unlike more dispersed GO, which may partially hinder substrate diffusion.

Complementing these dispersion- and charge-dependent effects, hydrophobic and π–π stacking interactions also contribute to enzyme–GRM binding. Proteins often adsorb preferentially to graphitic or reduced graphene surfaces via hydrophobic interactions, complemented by van der Waals forces and polar interactions (e.g., hydrogen bonding; Rohit et al., 2025; Srivastava, 2020), as demonstrated for the nonenzymatic protein avidin (Macwan et al., 2017). π–π stacking between aromatic amino acid residues (e.g., tryptophan, phenylalanine) and the basal plane of graphene is similarly well established in both theoretical and experimental studies (Rajesh et al., 2009). Molecular dynamics simulations suggest that defects on graphene surfaces can promote partial protein unfolding through a combination of hydrophobic and π–π interactions (Gu et al., 2019). These forces are expected to be more relevant for rGO and FLG due to their lower oxidation and larger graphitic domains, whereas GO engages proteins predominantly via electrostatic attraction and hydrogen bonding, forming weak but dynamically exchanging adsorption complexes (Malik et al., 2020) (Table 2).

Although our assays did not directly isolate hydrophobic or π–π contributions, the overall pattern of inhibition suggests that electrostatic adsorption is the principal mechanism driving LiP sequestration in this system. Only GO, characterized by its strong negative charge and dense oxygen functionalization, substantially reduced free LiP and product formation. In contrast, rGO and FLG, despite their greater hydrophobicity, higher π–π interaction potential, and distinct geometries, produced minimal inhibition except at the highest doses. This divergence indicates that hydrophobic, π–π, and van der Waals forces alone are insufficient to cause measurable activity loss under our conditions. Taken together, the data support a multifactorial interaction landscape across all GRMs, but one in which surface charge dominates functional outcomes.

The progressive reduction in oxygen-containing groups from GO → rGO → FLG (Table 1) did not strengthen inhibition, even though it increases hydrophobicity and graphitic character. Instead, at low and

Table 2 Properties of graphene-related materials governing interaction forces with enzymes.

GRM	Oxidation/ functional groups	Surface charge (ζ-potential)	Hydro-phobicity	π–π Potential	Size/geome-try/layering	Dispersion/ aggregation	Dominant interaction mechanisms
GO	High (–OH, –COOH, –CO)	Highly negative	Low	Low	Small, few-layer sheets	High dispersion; low aggregation	Electrostatic + H-bonding
rGO	Medium (residual –OH, –COOH; partial sp^2 restoration)	Moderately negative	Medium	Medium	Medium size, few layers; moderate aggregation	Moderate dispersion; moderate aggregation	Electrostatic > hydrophobic/ π–π/van der Waals
FLG	Low (mostly sp^2 carbon; minimal oxygen groups)	Moderately negative	High	High	Large, multilayer stacks	Low dispersion; strong aggregation	Hydrophobic/ π–π/van der Waals > electrostatic

Note. FLG = few-layer graphene; rGO = reduced graphene oxide; GO = graphene oxide.

moderate concentrations, only GO's highly anionic surface produced a significant reduction in soluble LiP; catalytic output, however, remained unaffected. This decoupling of adsorption from inhibition shows that sequestration alone does not necessarily inactivate the enzyme. It is also important to note that, although GO exhibited the strongest effects overall, all three GRMs influenced enzyme behavior at the highest concentration tested. Overall, only when sufficient enzyme becomes trapped away from the soluble phase does the catalytic capacity fall below the threshold required to sustain reaction rates. Thus, the observed activity patterns are consistent with a sequestration-driven loss of soluble enzyme, rather than direct catalytic inactivation. Because reactions were quantified only after incubation and physical removal of GRMs, we could not monitor reaction progress in real time and therefore cannot infer specific inhibition modes or derive kinetic parameters. Future studies employing complementary methods, such as fluorescence-based real-time assays, contact angle measurements, or atomic force microscopy (AFM), would enable more quantitative resolution of kinetics, hydrophobic, geometric, and adsorption-mediated contributions.

However, the shifts in zeta potential upon enzyme addition most strongly support the sequestration mechanism, indicating the formation of a protein corona at the enzyme–GRM interface. Such a corona can modify the physicochemical properties of both components, impose structural or conformational stress on LiP, and modulate accessibility to the catalytic site (Mishra et al., 2021; Quagliarini et al., 2023; Yang et al., 2021). Within this framework, the protein corona constitutes a dynamic, potentially reversible interface capable of attenuating enzymatic activity without fully suppressing catalysis (Saptarshi et al., 2013). When in environmental compartments, GRMs could acquire a dynamic "eco-corona," similar in principle to the protein corona but composed of naturally secreted enzymes and natural organic matter (NOM; e.g., from humic substances). Such coronas have been shown to strongly adsorb onto nanoparticle surfaces, influencing aggregation, surface charge, reactivity, and ecotoxicological performance (Chowdhury et al., 2014; Das et al., 2023).

Environmental and biotechnological implications

Our findings on the differential, charge-dependent interactions between GRMs and ligninolytic enzymes have significant implications for environmental management and biotechnology. Graphene-related materials are increasingly explored for applications such as water purification and soil remediation due to their high surface area and adsorptive capacities (Peña-Álvarez et al., 2024; Zubair et al., 2024), and they are also proposed as robust carriers for enzyme immobilization (Elgoyhen & Tomovska, 2025). This work highlights a critical "dual-role" paradox: the same properties that make GO an effective adsorbent can also lead to nontarget sequestration and inhibition of essential endogenous enzymes, such as LiP. This presents a challenge for environmental risk assessment (ERA), because the accumulation of GRMs in the environment could disrupt natural biogeochemical processes like carbon cycling that depend on fungal enzyme activity (Chung et al., 2015). However, the observation that LiP is inhibited at its positively charged buffer pH (3.2), whereas Lac is unaffected at its negatively charged buffer pH (4.5), provides a specific, predictable mechanism that should inform regulatory exposure models and Safe-by-Design (SbD) strategies. Designing nanomaterials with tunable surface chemistry and charge could, for instance, mitigate or harness electrostatic interactions (Hu et al., 2022; Li et al., 2024; Xu et al., 2021).

It is important to note that LiP retained partial catalytic activity despite reduced product formation, whereas Lac activity was largely unaffected by all tested GRMs. This is significant because laccases are widespread among fungi and bacteria and provide an alternative enzymatic pathway for pollutant transformation (Agarwal et al., 2022; Viswanath et al., 2014). Other ligninolytic enzymes, such as manganese peroxidase (MnP), have also been reported to interact with oxidized carbon nanomaterials, exhibiting altered function (such as inhibition due to co-factor chelation or altered kinetics) in environmental contexts (Zhang et al., 2014). These observations align with the principle of microbial infallibility: when exposed to emergent contaminants, certain enzymes may be partially inhibited, as observed with GRMs, and yet microorganisms can exploit alternative pathways to achieve degradation. In this context, GRMs in the environment are unlikely to entirely escape biotransformation, because microbial communities can deploy a diverse enzymatic arsenal that overcomes potential limitations due to charge-driven sequestration.

Conclusions and future directions

This study provides new insights on how graphene-related nanomaterials interact with fungal biodegradative enzymes, revealing enzyme- and material-specific effects. Lignin peroxidase exhibited concentration-dependent inhibition, particularly in the presence of

GO, whereas laccase remained largely unaffected. Notably, LiP retained partial catalytic activity despite sequestration, demonstrating that inhibitory interactions do not fully abolish enzymatic function. The observed patterns indicate that electrostatic adsorption is the primary driver of enzyme sequestration, with material dispersibility, aggregation, and surface functionalization further modulating interactions. These results emphasize that enzyme identity, GRM properties, and the physicochemical environment jointly determine the extent of interaction, and that conclusions drawn from one enzyme–GRM system cannot be generalized without experimental validation.

Future research should explore how environmental conditions, including pH, ionic strength, and temperature, influence enzyme–GRM interactions, as well as the structural impacts on sequestered enzymes using techniques such as fluorescence spectroscopy and circular dichroism. Additionally, assessing interactions in environmentally relevant contexts, including natural organic matter and microbial consortia, is critical to better understand GRM fate, biotransformation, and ecological effects. These findings are relevant for environmental risk assessment and sustainable nanomaterial design. They highlight that GRMs can selectively modulate enzymatic activity, potentially influencing biogeochemical processes in natural and engineered systems. Understanding these mechanisms is essential for predicting environmental outcomes and for designing strategies that exploit fungal oxidative enzymes for GRM remediation or other biotechnological applications.

Supplementary material

Supplementary material is available online at *Integrated Environmental Assessment and Management*.

Data availability

The data underlying this article will be shared on reasonable request to the corresponding author.

Author contributions

Humberto Castillo González (Conceptualization, Data curation, Formal analysis, Investigation, Methodology, Validation, Visualization, Writing—original draft, Writing—review & editing), Fabio Candotto Carniel (Conceptualization, Methodology, Resources, Supervision, Validation, Writing—review & editing), Mario Mardirossian (Conceptualization, Methodology, Resources, Validation, Writing—review & editing), Ester Vazquez (Funding acquisition, Resources, Validation, Writing—review & editing), Maurizio Prato (Funding acquisition, Resources, Validation, Writing—review & editing), and Mauro Tretiach (Conceptualization, Funding acquisition, Methodology, Project administration, Resources, Supervision, Validation, Writing—review & editing)

Funding

This work was supported by the European Union scientific research initiative “Graphene Flagship” Core 3 (grant agreement no. 881603).

Conflicts of interest

None declared.

Acknowledgments

The authors thank Alessia Norbedo and Andrea Bogo (University of Trieste, Italy) for their assistance with the use of equipment, and Lorenzo Fortuna (University of Trieste, Italy) for the insightful discussions.

References

Agarwal, N., Solanki, V. S., Gacem, A., Hasan, M. A., Pare, B., Srivastava, A., Singh, A., Yadav, V. K., Yadav, K. K., Lee, C., Lee, W., Chaiprapat, S., & Jeon, B. H. (2022). Bacterial laccases as biocatalysts for the remediation of environmental toxic pollutants: A green and eco-friendly approach—A review. *Water*, *14*, 4068. https://doi.org/10.3390/w14244068

Ali, J., Li, Y., Shang, E., Wang, X., Zhao, J., Mohiuddin, M., & Xia, X. (2023). Aggregation of graphene oxide and its environmental implications in the aquatic environment. *Chinese Chemical Letters*, *34*, 107327. https://doi.org/10.1016/j.cclet.2022.03.050

Barnhart-Dailey, M. C., Ye, D., Hayes, D. C., Maes, D., Simoes, C. T., Appelhans, L., Carroll-Portillo, A., Kent, M. S., & Timlin, J. A. (2019). Internalization and accumulation of model lignin breakdown products in bacteria and fungi. *Biotechnology for Biofuels*, *12*, 175. https://doi.org/10.1186/s13068-019-1494-8

Boulanger, N., Kuzenkova, A. S., Iakunkov, A., Nordenström, A., Romanchuk, A. Y., Trigub, A. L., Zasimov, P. V., Prodana, M., Enachescu, M., Bauters, S., Amidani, L., Kvashnina, K. O., Kalmykov, S. N., & Talyzin, A. V. (2022). High surface area “3D graphene oxide” for enhanced sorption of radionuclides. *Advanced Materials Interfaces*, *9*, 2200510. https://doi.org/10.1002/admi.202200510

Candotto Carniel, F., Fortuna, L., Zanelli, D., Garrido, M., Vázquez, E., González, V. J., Prato, M., & Tretiach, M. (2021). Graphene environmental biodegradation: Wood degrading and saprotrophic fungi oxidize few-layer graphene. *Journal of Hazardous Materials*, *414*, 125553. https://doi.org/10.1016/j.jhazmat.2021.125553

Caorsi, G., Candotto Carniel, F., Légnani, M., Flahaut, E., González, V. J., Vázquez, E., Prato, M., & Tretiach, M. (2025). Applicability of the OECD Test Guideline 201 to graphene-related materials: Dispersion stability matters. *Ecotoxicology and Environmental Safety*, *292*, 117888. https://doi.org/10.1016/j.ecoenv.2025.117888

Chen, L., Batchelor-McAuley, C., Rasche, B., Johnston, C., Hindle, N., & Compton, R. G. (2020). Surface area measurements of graphene and graphene oxide samples: Dopamine adsorption as a complement or alternative to methylene blue? *Applied Materials Today*, *18*, 100506. https://doi.org/10.1016/j.apmt.2019.100506

Chowdhury, I., Duch, M. C., Mansukhani, N. D., Hersam, M. C., & Bouchard, D. (2014). Interactions of graphene oxide nanomaterials with natural organic matter and metal oxide surfaces. *Environmental Science & Technology*, *48*, 9382–9390. https://doi.org/10.1021/es5020828

Chung, H., Kim, M. J., Ko, K., Kim, J. H., Kwon, H.-A., Hong, I., Park, N., Lee, S. W., & Kim, W. (2015). Effects of graphene oxides on soil enzyme activity and microbial biomass. *Science of the Total Environment*, *514*, 307–313. https://doi.org/10.1016/j.scitotenv.2015.01.077

Das, P., Penton, C. R., Westerhoff, P., & Perreault, F. (2023). Prospects of 2D graphene nanomaterials in plant-based agriculture and their fate in terrestrial soil: A critical review. *Environmental Science: Nano*, *10*, 2936–2956. https://doi.org/10.1039/d3en00511a

Ding, X., Pu, Y., Tang, M., & Zhang, T. (2022). Environmental and health effects of graphene-family nanomaterials: Potential release pathways, transformation, environmental fate and health risks. *Nano Today*, *42*, 101379. https://doi.org/10.1016/j.nantod.2022.101379

Elgoyhen, J., & Tomovska, R. (2025). Advanced technologies for wastewater treatment: Graphene-based catalysts. *Molecules*, *30*, 3405. https://doi.org/10.3390/molecules30163405

Evariste, L., Braylé, P., Mouchet, F., Silvestre, J., Gauthier, L., Flahaut, E., Pinelli, E., & Barret, M. (2021). Graphene-based nanomaterials modulate internal biofilm interactions and microbial diversity. *Frontiers in Microbiology*, *12*, 623853. https://doi.org/10.3389/fmicb.2021.623853

Fadil, Y., Dinh, L. N. M., Yap, M. O. Y., Kuchel, R. P., Yao, Y., Omura, T., Aregueta-Robles, U. A., Song, N., Huang, S., Jasinski, F., Thickett, S. C., Minami, H., Agarwal, V., & Zetterlund, P. B. (2019). Ambient-temperature waterborne polymer/rGO nanocomposite films: Effect of rGO distribution on electrical conductivity. *ACS Applied Materials & Interfaces*, *11*, 48450–48458. https://doi.org/10.1021/acsami.9b19183

Fan, J., Grande, C. D., & Rodrigues, D. F. (2017). Biodegradation of graphene oxide–polymer nanocomposite films in wastewater. *Environmental Science: Nano*, *4*, 1808–1816. https://doi.org/10.1039/C7EN00396J

Fojtů, M., Teo, W. Z., & Pumera, M. (2017). Environmental impact and potential health risks of 2D nanomaterials. *Environmental Science: Nano*, *4*, 1617–1633. https://doi.org/10.1039/C7EN00401J

Fortuna, L., Garrido, M., Castillo-Gonzalez, H., Zanelli, D., Martín, C., Candotto Carniel, F., Vázquez, E., Prato, M., Bianco, A., & Tretiach, M. (2023). Graphene oxide degradation by a white-rot fungus occurs in spite of lignin peroxidase inhibition. *Environmental Science: Nano*, *10*, 2286–2298. https://doi.org/10.1039/d3en00072a

González, V. J., Rodríguez, A. M., Payo, I., & Vázquez, E. (2020). Mechanochemical preparation of piezoelectric nanomaterials: BN, MoS2 and WS2 two-dimensional materials and their glycine cocrystals. *Nanoscale Horizons*, *5*, 331–335. https://doi.org/10.1039/C9NH00494G

González-Domínguez, J. M., León, V., Lucío, M. I., Prato, M., & Vázquez, E. (2018). Production of ready-to-use few-layer graphene in aqueous suspensions. *Nature Protocols*, *13*, 495–506. https://doi.org/10.1038/nprot.2017.142

Goodrum, R., Weldekidan, H., Li, H., Mohanty, A. K., & Misra, M. (2024). Graphene-based nanostructures from green processes and their applications in biomedical sensors. *Advanced Industrial and Engineering Polymer Research*, *7*, 37–53. https://doi.org/10.1016/j.aiepr.2023.03.001

Goodwin, D. G., Adeleye, A. S., Sung, L., Ho, K. T., Burgess, R. M., & Petersen, E. J. (2018). Detection and quantification of graphene family nanomaterials in the environment. *Environmental Science & Technology*, *52*, 4491–4513. https://doi.org/10.1021/acs.est.7b04938

Gu, Z., Song, W., Chen, S. H., Li, B., Li, W., & Zhou, R. (2019). Defect-assisted protein HP35 denaturation on graphene. *Nanoscale*, *11*, 19362–19369. https://doi.org/10.1039/C9NR01143A

Gumustas, M., Sengel-Turk, C. T., Gumustas, A., Ozkan, S. A., & Uslu, B. (2017). Effect of polymer-based nanoparticles on the assay of antimicrobial drug delivery systems. In A. A. El Kharraz & A. M. R. Pinto (Eds.), *Multifunctional systems for combined delivery, biosensing and diagnostics* (pp. 67–108). Elsevier. https://doi.org/10.1016/B978-0-323-52725-5.00005-8

Guo, F., Creighton, M., Chen, Y., Hurt, R., & Külaots, I. (2014). Porous structures in stacked, crumpled and pillared graphene-based 3D materials. *Carbon*, *66*, 476–484. https://doi.org/10.1016/j.carbon.2013.09.024

Henriques, P. C., Pereira, A. T., Pires, A. L., Pereira, A. M., Magalhães, F. D., & Gonçalves, I. C. (2020). Graphene surfaces interaction with proteins, bacteria, mammalian cells, and blood constituents: The impact of graphene platelet oxidation and thickness. *ACS Applied Materials & Interfaces*, *12*, 21020–21035. https://doi.org/10.1021/acsami.9b21841

Hong, H., & Nowack, B. (2024). Form-specific prospective environmental risk assessment of graphene-based materials in European freshwater. *Environmental Science & Technology*, *58*, 21750–21759. https://doi.org/10.1021/acs.est.4c05153

Houtman, C. J., Maligaspe, E., Hunt, C. G., Fernández-Fueyo, E., Martínez, A. T., & Hammel, K. E. (2018). Fungal lignin peroxidase does not produce the veratryl alcohol cation radical as a diffusible ligninolytic oxidant. *The Journal of Biological Chemistry*, *293*, 4702–4712. https://doi.org/10.1074/jbc.RA117.001153

Hu, H., Wen, W., & Ou, J. Z. (2022). Construction of adsorbents with graphene and its derivatives for wastewater treatment: A review. *Environmental Science: Nano*, *9*, 3226–3276. https://doi.org/10.1039/D2EN00248E

Islam, F., Wang, J., Tahmasebi, A., Wang, R., Moghtaderi, B., & Yu, J. (2021). Microwave-assisted coal-derived few-layer graphene as an anode material for lithium-ion batteries. *Materials*, *14*, 6468. https://doi.org/10.3390/ma14216468

Jiang, Y., Raliya, R., Fortner, J. D., & Biswas, P. (2016). Graphene oxides in water: Correlating morphology and surface chemistry with aggregation behavior. *Environmental Science & Technology*, *50*, 6964–6973. https://doi.org/10.1021/acs.est.6b00810

Kantharaj, P., Boobalan, B., Sooriamuthu, S., & Mani, R. (2017). Lignocellulose degrading enzymes from fungi and their industrial applications. *International Journal of Current Research and Review*, *9*, 1–13. https://doi.org/10.7324/ijcrr.2017.9211

Karaphun, A., Phrompet, C., Tuichai, W., Chanlek, N., Sriwong, C., & Ruttanapun, C. (2021). The influence of annealing on a large specific surface area and enhancing electrochemical properties of reduced graphene oxide to improve the performance of the active electrode of supercapacitor devices. *Materials Science and Engineering: B*, *264*, 114941. https://doi.org/10.1016/j.mseb.2020.114941

Keller, A. A., & Lazareva, A. (2014). Predicted releases of engineered nanomaterials: From global to regional to local. *Environmental Science & Technology Letters*, *1*, 65–70. https://doi.org/10.1021/ez400106t

Kenry, & Lim, C. T. (2017). Biocompatibility and nanotoxicity of layered two-dimensional nanomaterials. *ChemNanoMat*, *3*, 5–16. https://doi.org/10.1002/cnma.201600290

Kumar, A., & Chandra, R. (2020). Ligninolytic enzymes and mechanisms for degradation of lignocellulosic waste in the environment. *Heliyon*, *6*, e03170. https://doi.org/10.1016/j.heliyon.2020.e03170

Kumar, S., & Parekh, S. H. (2020). Linking graphene-based material physicochemical properties with molecular adsorption, structure and cell fate. *Communications Chemistry*, *3*, 8. https://doi.org/10.1038/s42004-019-0254-9

Kumari, S., Sharma, P., Ghosh, D., Shandilya, M., Rawat, P., Hassan, M. I., Moulick, R. G., Bhattacharya, J., Srivastava, C., & Majumder, S. (2020). Time-dependent study of the graphene oxide–trypsin adsorption interface and visualization of nano-protein corona. *International Journal of Biological Macromolecules*, *163*, 2259–2269. https://doi.org/10.1016/j.ijbiomac.2020.09.099

Lee, S., Eom, S. H., Chung, J. S., & Hur, S. H. (2013). Large-scale production of high-quality reduced graphene oxide. *Chemical Engineering Journal*, *233*, 297–304. https://doi.org/10.1016/j.cej.2013.08.050

Li, G., Du, R., Cao, Z., Li, C., Xue, J., Ma, X., & Wang, S. (2024). Research progress in graphene-based adsorbents for wastewater treatment: Preparation, adsorption properties and mechanisms for inorganic and organic pollutants. *C*, *10*, 78. https://doi.org/10.3390/c10030078

Liu, Z., Navik, R., Tan, H., Xiang, Q., Goto, M., Ibarra, R. M., Zhao., & Wahyudiono, Y.. (2022a). Graphene-based materials prepared by supercritical fluid technology and applications in energy storage. *The Journal of Supercritical Fluids*, *188*, 105672. https://doi.org/10.1016/j.supflu.2022.105672

Liu, Z., Zhao, J., Lu, K., Wang, Z., Yin, L., Zheng, H., Wang, X., Mao, L., & Xing, B. (2022b). Biodegradation of graphene oxide by insects (Tenebrio molitor larvae): Role of the gut microbiome and enzymes. *Environmental Science & Technology*, *56*, 16737–16747. https://doi.org/10.1021/acs.est.2c03342

Macwan, I., Khan, M. D. H., Aphale, A., Singh, S., Liu, J., Hingorani, M., & Patra, P. (2017). Interactions between avidin and graphene for development of a biosensing platform. *Biosensors & Bioelectronics*, *89*, 326–333. https://doi.org/10.1016/j.bios.2016.07.024

Madenli, Ö., & Deveci, E. Ü. (2023). Evaluation of potential environmental risks of graphene-based materials by examining the effect of rGO on the microbial activity of *Phanerochaete chrysosporium*. *International Journal of Advances in Engineering and Pure Sciences*, *35*, 177–182. https://doi.org/10.7240/jeps.1174562

Malik, S. A., Mohanta, Z., Srivastava, C., & Atreya, H. S. (2020). Modulation of protein–graphene oxide interactions with varying degrees of oxidation. *Nanoscale Advances*, *2*, 1904–1912. https://doi.org/10.1039/C9NA00807A

Malisz, K., & Świeczko-Żurek, B. (2023). Graphene production and biomedical applications: A review. *Crystals*, *13*, 1413. https://doi.org/10.3390/cryst13101413

Martín-De-Lucía, I., Campos-Mañas, M. C., Agüera, A., Leganés, F., Fernández-Piñas, F., & Rosal, R. (2018). Combined toxicity of graphene oxide and wastewater to the green alga *Chlamydomonas reinhardtii*. *Environmental Science: Nano*, *5*, 1729–1744. https://doi.org/10.1039/C8EN00138C

Martinez, D. V., Rodriguez, A., Juarros, M. A., Martinez, E. J., Alam, T. M., Sale, K. L., Kent, M. S., Simmons, B. A., & Singer, S. W. (2022). Depolymerization of lignin for biological conversion through sulfonation and a chelator-mediated Fenton reaction. *Green Chemistry*, *24*, 1627–1643. https://doi.org/10.1039/D1GC03854K

Mishra, R. K., Ahmad, A., Vyawahare, A., Alam, P., Khan, T. H., & Khan, R. (2021). Biological effects of formation of protein corona onto nanoparticles. *International Journal of Biological Macromolecules*, *175*, 1–18. https://doi.org/10.1016/j.ijbiomac.2021.01.152

Mokhtari-Farsani, A., Hasany, M., Lynch, I., & Mehrali, M. (2022). Biodegradation of carbon-based nanomaterials: The importance of biomolecular corona consideration. *Advanced Functional Materials*, *32*211, 220. https://doi.org/10.1002/adfm.202105649

Németh, I., László, K., Bulátkó, A., Vaszita, E., & Molnár, M. (2023). Ecotoxicity assessment of graphene oxides using test organisms from three hierarchical trophic levels to evaluate their potential environmental risk. *Nanomaterials*, *13*, 2858. https://doi.org/10.3390/nano13212858

Nidamanuri, N., Li, Y., Li, Q., & Dong, M. (2020). Graphene- and graphene oxide–based membranes for gas separation. *Engineered Science*, *9*, 3–16. https://doi.org/10.30919/es8d128906

Ortiz-Anaya, I., & Nishina, Y. (2024). Refined surface area determination of graphene oxide using methylene blue as a probe molecule: A comparative approach. *Bulletin of the Chemical Society of Japan*, *97*, 1250–1259. https://doi.org/10.1093/bulcsj/uoae118

Peña-Álvarez, V., Baragaño, D., Prosenkov, A., Gallego, J. R., & Peláez, A. I. (2024). Assessment of co-contaminated soil amended by graphene oxide: Effects on pollutants, microbial communities and soil health. *Ecotoxicology and Environmental Safety*, *272*, 116015. https://doi.org/10.1016/j.ecoenv.2024.116015

Purkait, T., Singh, G., Singh, M., Kumar, D., & Dey, R. S. (2017). Large area few-layer graphene with scalable preparation from waste biomass for high-performance supercapacitor. *Scientific Reports*, *7*, 15239. https://doi.org/10.1038/s41598-017-15463-w

Qu, Y., Wang, J., Ma, Q., Shen, W., Pei, X., You, S., Yin, Q., & Li, X. (2018). A novel environmental fate of graphene oxide: Biodegradation by a bacterium *Labrys* sp. WJW to support growth. *Water Research*, *143*, 260–269. https://doi.org/10.1016/j.watres.2018.03.070

Quagliarini, E., Pozzi, D., Cardarelli, F., & Caracciolo, G. (2023). The influence of protein corona on graphene oxide: Implications for biomedical theranostics. *Journal of Nanobiotechnology*, *21*, 267. https://doi.org/10.1186/s12951-023-02030-x

Rajesh, C., Majumder, C., Mizuseki, H., & Kawazoe, Y. (2009). A theoretical study on the interaction of aromatic amino acids with graphene and single-walled carbon nanotubes. *The Journal of Chemical Physics*, *130*, 124911. https://doi.org/10.1063/1.3079096

Rohit, Bharadwaj, R., Roy, C., Ghosh, S., & Kumar, S. (2025). Surface potential modulates fibronectin adsorption and molecular interaction on graphene-based materials. *Biointerphases*, *20*, 031001. https://doi.org/10.1116/6.0004504

Saptarshi, S. R., Duschl, A., & Lopata, A. L. (2013). Interaction of nanoparticles with proteins: Relation to bio-reactivity of the nanoparticle. *Journal of Nanobiotechnology*, *11*, 26. https://doi.org/10.1186/1477-3155-11-26

Shams, M., Mansukhani, N., Hersam, M. C., Bouchard, D., & Chowdhury, I. (2023). Environmentally sustainable implementations of two-dimensional nanomaterials. *Frontiers in Chemistry*, *11*, 1132233. https://doi.org/10.3389/fchem.2023.1132233

Shnoudeh, A. J., Hamad, I., Abdo, R. W., Qadumii, L., Jaber, A. Y., Surchi, H. S., & Alkelany, S. Z. (2019). Synthesis, characterization, and applications of metal nanoparticles. In S. R. Thomas, J. K. B. Mathew, & M. S. Shalaby (Eds.), *Biomaterials and bionanotechnology* (pp. 527–612). Elsevier. https://doi.org/10.1016/B978-0-12-814427-5.00015-9

Srivastava, R. (2020). Interactions, electronic and optical properties of nanographene–peptide complexes: A theoretical study. *RSC Advances*, *10*, 38654–38662. https://doi.org/10.1039/D0RA07961H

Van Khai, T., Kwak, D. S., Kwon, Y. J., Cho, H. Y., Huan, T. N., Chung, H., Ham, H., Lee, C., Dan, N. V., Tung, N. T., & Kim, H. W. (2013). Direct production of highly conductive graphene with a low oxygen content by a microwave-assisted solvothermal method. *Chemical Engineering Journal*, *232*, 346–355. https://doi.org/10.1016/j.cej.2013.07.123

Viswanath, B., Rajesh, B., Janardhan, A., Kumar, A. P., & Narasimha, G. (2014). Fungal laccases and their applications in bioremediation. *Enzyme Research*, *2014*, 163242. https://doi.org/10.1155/2014/163242

Wang, S., Minami, D., & Kaneko, K. (2015). Comparative pore structure analysis of highly porous graphene monoliths treated at different temperatures with adsorption of N2 at 77.4 K and Ar at 87.3 K and 77.4 K. *Microporous and Mesoporous Materials*, *209*, 72–78. https://doi.org/10.1016/j.micromeso.2015.01.014

Wojciechowska, O., Costabile, A., & Kujawska, M. (2023). The gut microbiome meets nanomaterials: Exposure and interplay with graphene nanoparticles. *Nanoscale Advances*, *5*, 6349–6364. https://doi.org/10.1039/d3na00696d

Xie, J., Ming, Z., Li, H., Yang, H., Yu, B., Wu, R., Liu, X., Bai, Y., & Yang, S. T. (2016). Toxicity of graphene oxide to white-rot fungus *Phanerochaete chrysosporium*. *Chemosphere*, *151*, 324–331. https://doi.org/10.1016/j.chemosphere.2016.02.097

Xu, K., Wang, B., Si, C., Lin, C., Zheng, R., & Zheng, Y. (2021). Surface modulation of graphene oxide for amidase immobilization with high loadings for efficient biocatalysis. *Biomolecules*, *11*, 1399. https://doi.org/10.3390/biom11101399

Yang, H., Feng, S., Ma, Q., Ming, Z., Bai, Y., Chen, L., & Yang, S. T. (2018). Influence of reduced graphene oxide on the growth, structure and decomposition activity of white-rot fungus *Phanerochaete*

chrysosporium. *RSC Advances*, *8*, 5026–5033. https://doi.org/10.1039/C7RA12364G

Yang, H., Wu, X., Ma, Q., Yilihamu, A., Yang, S., Zhang, Q., Feng, S., & Yang, S. T. (2019). Fungal transformation of graphene by white-rot fungus *Phanerochaete chrysosporium*. *Chemosphere*, *216*, 9–18. https://doi.org/10.1016/j.chemosphere.2018.10.115

Yang, Y., Han, P., Xie, X., Yin, X., Duan, G., & Wen, L. (2021). Protein corona reduced graphene oxide cytotoxicity by inhibiting endocytosis. *Colloid and Interface Science Communications*, *45*, 100514. https://doi.org/10.1016/j.colcom.2021.100514

Ye, N., Wang, Z., Wang, S., & Peijnenburg, W. J. G. M. (2018). Toxicity of mixtures of zinc oxide and graphene oxide nanoparticles to aquatic organisms of different trophic levels: Particles outperform dissolved ions. *Nanotoxicology*, *12*, 423–438. https://doi.org/10.1080/17435390.2018.1458342

Yu, W., Sisi, L., Haiyan, Y., & Jie, L. (2020). Progress in the functional modification of graphene/graphene oxide: A review. *RSC Advances*, *10*, 15328–15345. https://doi.org/10.1039/d0ra01068e

Zhang, C., Chen, S., Alvarez, P. J. J., & Chen, W. (2015). Reduced graphene oxide enhances horseradish peroxidase stability by serving as radical scavenger and redox mediator. *Carbon*, *94*, 531–538. https://doi.org/10.1016/j.carbon.2015.07.036

Zhang, C., Chen, W., & Alvarez, P. J. J. (2014). Manganese peroxidase degrades pristine but not surface-oxidized (carboxylated) single-walled carbon nanotubes. *Environmental Science & Technology*, *48*, 7918–7923. https://doi.org/10.1021/es5011175

Zhang, J., Lu, X., Shi, C., Yan, B., Gong, L., Chen, J., Xiang, L., Xu, H., Liu, Q., & Zeng, H. (2019). Unraveling the molecular interaction mechanism between graphene oxide and aromatic organic compounds with implications on wastewater treatment. *Chemical Engineering Journal*, *358*, 842–849. https://doi.org/10.1016/j.cej.2018.10.064

Zhang, M., Fu, G., Shi, W., Feng, X., Lens, P. N. L., & Zhang, B. (2024). Microbial response to the chronic toxicity effect of graphene and graphene oxide nanomaterials within aerobic granular sludge systems. *Journal of Hazardous Materials*, *477*, 135350. https://doi.org/10.1016/j.jhazmat.2024.135350

Zhang, W., Wang, W., Wang, J., Shen, G., Yuan, Y., Yan, L., Tang, H., & Wang, W. (2021). Isolation and characterization of a novel laccase for lignin degradation, LacZ1. *Applied and Environmental Microbiology*, *87*, e01355-21. https://doi.org/10.1128/AEM.01355-21

Zhang, X., Cao, H., Wang, H., Zhao, J., Gao, K., Qiao, J., Li, J., & Ge, S. (2022). The effects of graphene-family nanomaterials on plant growth: A review. *Nanomaterials*, *12*, 936. https://doi.org/10.3390/nano12060936

Zhao, J., Lin, M., Wang, Z., Cao, X., & Xing, B. (2021). Engineered nanomaterials in the environment: Are they safe? *Critical Reviews in Environmental Science and Technology*, *51*, 1443–1478. https://doi.org/10.1080/10643389.2020.1764279

Zubair, M., Roopesh, M. S., & Ullah, A. (2024). Challenges and prospects: Graphene oxide–based materials for water remediation including metal ions and organic pollutants. *Environmental Science: Nano*, *11*, 3693–3720. https://doi.org/10.1039/D4EN00143E

Integrated Environmental Assessment and Management, 2026, 00, 1–12
https://doi.org/10.1093/inteam/vjag003
Original Article